Computation of Smooth Optical Flow in a Feedback Connected Analog Network

Alan Stocker *
Institute of Neuroinformatics
University and ETH Zürich
Winterthurerstrasse 190
8057 Zürich, Switzerland

Rodney Douglas
Institute of Neuroinformatics
University and ETH Zürich
Winterthurerstrasse 190
8057 Zürich, Switzerland

Abstract

In 1986, Tanner and Mead [1] implemented an interesting constraint satisfaction circuit for global motion sensing in aVLSI. We report here a new and improved aVLSI implementation that provides smooth optical flow as well as global motion in a two dimensional visual field. The computation of optical flow is an ill-posed problem, which expresses itself as the aperture problem. However, the optical flow can be estimated by the use of regularization methods, in which additional constraints are introduced in terms of a global energy functional that must be minimized. We show how the algorithmic constraints of Horn and Schunck [2] on computing smooth optical flow can be mapped onto the physical constraints of an equivalent electronic network.

1 Motivation

The perception of apparent motion is crucial for navigation. Knowledge of local motion of the environment relative to the observer simplifies the calculation of important tasks such as time-to-contact or focus-of-expansion. There are several methods to compute optical flow. They have the common problem that their computational load is large. This is a severe disadvantage for autonomous agents, whose computational power is restricted by energy, size and weight. Here we show how the global regularization approach which is necessary to solve for the ill-posed nature of computing optical flow, can be formulated as a local feedback constraint, and implemented as a physical analog device that is computationally efficient.

* correspondence to: alan@ini.phys.ethz.ch

2 Smooth Optical Flow

Horn and Schunck [2] defined optical flow in relation to the spatial and temporal changes in image brightness. Their model assumes that the total image brightness $E(x, y, t)$ does not change over time;

$$\frac{d}{dt}E(x, y, t) = 0. \tag{1}$$

Expanding equation (1) according to the chain rule of differentiation leads to

$$F \equiv \frac{\delta}{\delta x}E(x, y, t)u + \frac{\delta}{\delta y}E(x, y, t)v + \frac{\delta}{\delta t}E(x, y, t) = 0, \tag{2}$$

where $u = dx/dt$ and $v = dy/dt$ represent the two components of the local optical flow vector.

Since there is one equation for two unknowns at each spatial location, the problem is ill-posed, and there are an infinite number of possible solutions lying on the *constraint line* for every location (x, y). However, by introducing an additional constraint the problem can be regularized and a unique solution can be found.

For example, Horn and Schunck require the optical flow field to be smooth. As a measure of smoothness they choose the squares of of the spatial derivatives of the flow vectors,

$$S^2 = \left(\frac{\delta u}{\delta x}\right)^2 + \left(\frac{\delta u}{\delta y}\right)^2 + \left(\frac{\delta v}{\delta x}\right)^2 + \left(\frac{\delta v}{\delta y}\right)^2. \tag{3}$$

One can also view this constraint as introducing *a priori* knowledge: the closer two points are in the image space the more likely they belong to the projection of the same object. Under the assumption of rigid objects undergoing translational motion, this constraint implies that the points have the same, or at least very similar motion vectors. This assumption is obviously not valid at boundaries of moving objects, and so this algorithm fails to detect motion discontinuities [3].

The computation of smooth optical flow can now be formulated as the minimization problem of a global energy functional,

$$\iint \underbrace{F^2 + \lambda S^2}_{L}\, dx\, dy \longrightarrow min \tag{4}$$

with F and S^2 as in equation (2) and (3) respectively. Thus, we exactly apply the approach of *standard regularization theory* [4]:

$\mathbf{Ax} = \mathbf{y}$	y: data
$\mathbf{x} = \mathbf{A}^{-1}\mathbf{y}$	inverse problem, ill-posed
$\parallel \mathbf{Ax} - \mathbf{y} \parallel + \lambda \parallel \mathbf{P} \parallel = \min$	regularization

The regularization parameter, λ, controls the degree of smoothing of the solution and its closeness to the data. The norm, $\|\cdot\|$, is quadratic. A difference in our case is that $\mathbf{A}$ is not constant but depends on the data. However, if we consider motion on a discrete time-axis and look at snapshots rather than continuously changing images, $\mathbf{A}$ is *quasi-stationary*.[1] The energy functional (4) is convex and so, a simple numerical technique like gradient descent would be able to find the global minimum. To compute optical flow while preserving motion discontinuities one can modify the energy functional to include a binary line process that prevents smoothing over discontinuities [4]. However, such an functional will not be convex. Gradient descent methods would probably fail to find the global amongst all local minima and other methods have to be applied.

[1] In the aVLSI implementation this requires a much shorter settling time constant for the network than the brightness changes in the image.

3 A Physical Analog Model

3.1 Continuous space

Standard regularization problems can be mapped onto electronic networks consisting of conductances and capacitors [5]. Hutchinson et al. [6] showed how resistive networks can be used to compute optical flow and Poggio et al. [7] introduced electronic network solutions for second-order-derivative optic flow computation. However, these proposed network architectures all require complicated and sometimes negative conductances although Harris et al. [8] outlined a similar approach as proposed in this paper independently. Furthermore, such networks were not implemented practically, whereas our implementation with constant nearest neighbor conductances is intuitive and straightforward.
Consider equation (4):

$$L = L(u, v, \nabla u, \nabla v, x, y).$$

The *Lagrange function* L is sufficiently regular ($L \in C^2$), and thus it follows from calculus of variation that the solution of equation (4) also suffices the linear Euler-Lagrange equations

$$\begin{aligned} \lambda \nabla^2 u - E_x(E_x u + E_y v + E_t) &= 0 \\ \lambda \nabla^2 v - E_y(E_x u + E_y v + E_t) &= 0. \end{aligned} \quad (5)$$

The Euler-Lagrange equations are only necessary conditions for equation (4). The sufficient condition for solutions of equations (5) to be a weak minimum is the strong Legendre-condition, that is

$$L_{\nabla u \nabla u} > 0 \quad \text{and} \quad L_{\nabla v \nabla v} > 0,$$

which is easily shown to be true.

3.2 Discrete Space – Mapping to Resistive Network

By using a discrete five-point approximation of the Laplacian ∇^2 on a regular grid, equations (5) can be rewritten as

$$\begin{aligned} \lambda(u_{i+1,j} + u_{i-1,j} + u_{i,j+1} + u_{i,j-1} - 4u_{i,j}) - E_{x_{i,j}}(E_{x_{i,j}} u_{i,j} + E_{y_{i,j}} v_{i,j} + E_{t_{i,j}}) = 0 \\ \lambda(v_{i+1,j} + v_{i-1,j} + v_{i,j+1} + v_{i,j-1} - 4v_{i,j}) - E_{y_{i,j}}(E_{x_{i,j}} u_{i,j} + E_{y_{i,j}} v_{i,j} + E_{t_{i,j}}) = 0 \end{aligned} \quad (6)$$

where i and j are the indices for the sampling nodes. Consider a single node of the resistive network shown in Figure 1:

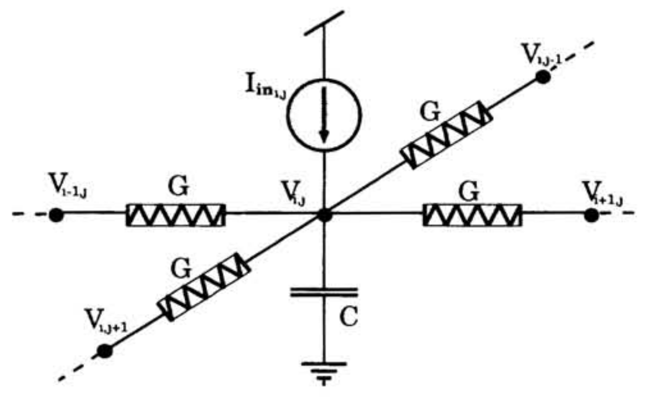

Figure 1: Single node of a resistive network.

From Kirchhoff's law it follows that

$$C\frac{dV_{i,j}}{dt} = G(V_{i+1,j} + V_{i-1,j} + V_{i,j+1} + V_{i,j-1} - 4V_{i,j}) + I_{in_{i,j}} \quad (7)$$

where $V_{i,j}$ represents the voltage and $I_{in_{i,j}}$ the input current. G is the conductance between two neighboring nodes and C the node capacitance.
In steady state, equation (7) becomes

$$G(V_{i+1,j} + V_{i-1,j} + V_{i,j+1} + V_{i,j-1} - 4V_{i,j}) + I_{in_{i,j}} = 0. \tag{8}$$

The analogy with equations (6) is obvious:

$$\begin{aligned} G &\longleftrightarrow \lambda \\ Iu_{in_{i,j}} &\longleftrightarrow -E_{x_{i,j}}(E_{x_{i,j}}u_{i,j} + E_{y_{i,j}}v_{i,j} + E_{t_{i,j}}) \\ Iv_{in_{i,j}} &\longleftrightarrow -E_{y_{i,j}}(E_{x_{i,j}}u_{i,j} + E_{y_{i,j}}v_{i,j} + E_{t_{i,j}}) \end{aligned} \tag{9}$$

To create the full system we use two parallel resistive networks in which the node voltages $U_{i,j}$ and $V_{i,j}$ represent the two components of the optical flow vector u and v. The input currents $Iu_{in_{i,j}}$ and $Iv_{in_{i,j}}$ are computed by a negative *recurrent feedback loop* modulated by the input data, which are the spatial and temporal intensity gradients.
Notice that the input currents are proportional to the deviation of the *local brightness constraint*: the less the local optical flow solution fits the data the higher the current $I_{in_{i,j}}$ will be to correct the solution and vice versa.
Stability and convergence of the network are guaranteed by Maxwell's minimum power principle [4, 9].

4 The Smooth Optical Flow Chip

4.1 Implementation

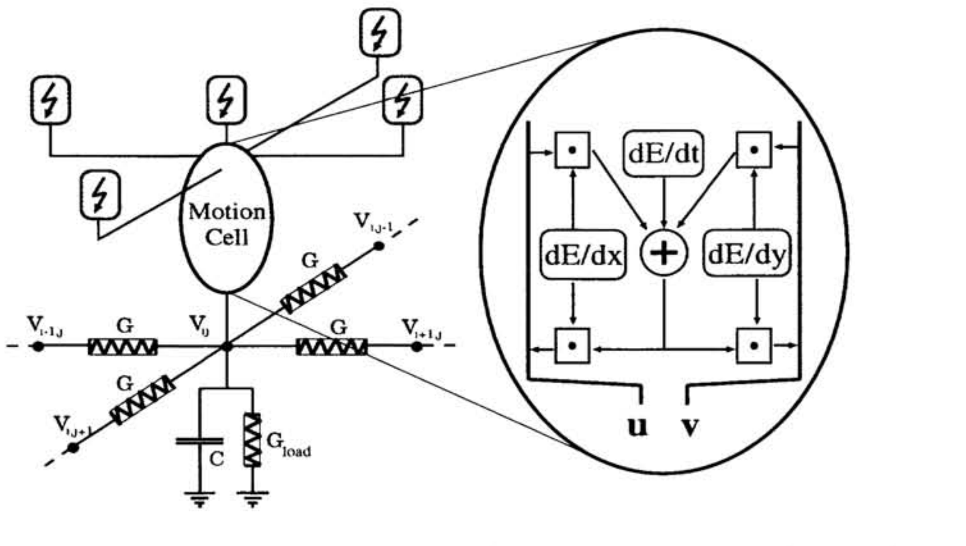

Figure 2: A single motion cell within the three layer network. For simplicity only one resistive network is shown.

The circuitry consists of three functional layers (Figure 2). The input layer includes an array of adaptive photoreceptors [10] and provides the derivatives of the image brightness to the second layer. The spatial gradients are the first-order linear approximation obtained by subtracting the two neighboring photoreceptor outputs. The second layer computes the input current to the third layer according to equations (9). Finally these currents are fed into the two resistive networks that report the optical flow components.
The schematics of the core of a single motion cell are drawn in Figure 3. The photoreceptor and the temporal differentiator are not shown as well as the other half of the circuitry that computes the y-component of the flow vector.

A few remarks are appropriate here: First, the two components of the optical flow vector have to be able to take on positive and negative values with respect to some reference potential. Therefore, a symmetrical circuit scheme is applied where the positive and negative (reference voltage) values are carried on separate signal lines. Thus, the actual value is encoded as the difference of the two potentials.

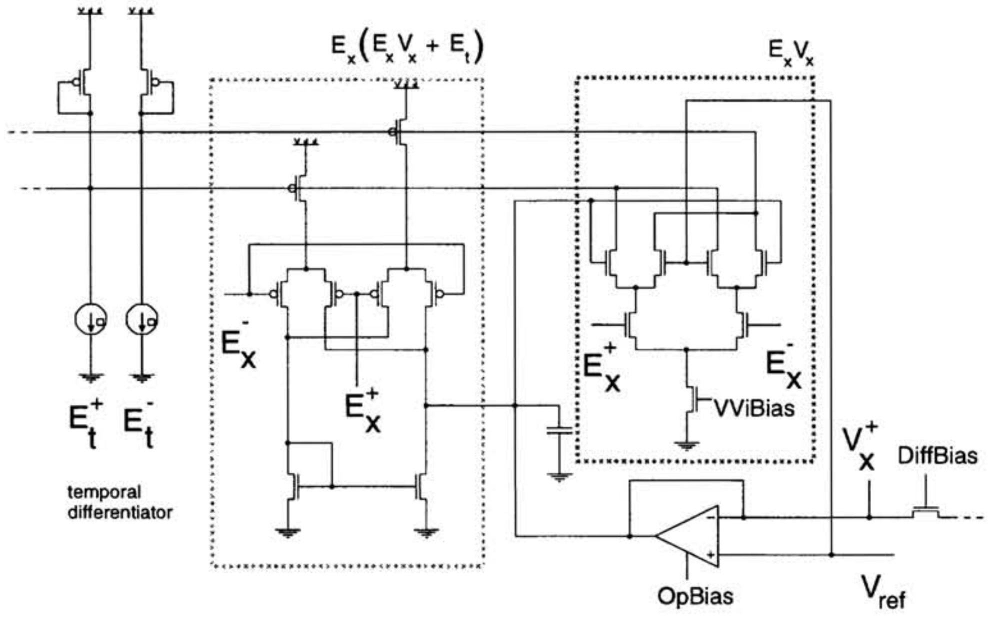

Figure 3: Cell core schematics; only the circuitry related to the computation of the x-component of the flow vector is shown.

Second, the limited linear range of the Gilbert multipliers leads to a narrow span of flow velocities that can be computed reliably. However, the tuning can be such that the operational range is either at high or very low velocities. Newer implementations are using modified multipliers with a larger linear range.
Third, consider a single motion cell (Figure 2). In principle, this cell would be able to satisfy the local constraint perfectly. In practice (see Figure 3), the finite output impedance of the p-type Gilbert multiplier slightly degrades this ideal solution by imposing an effective conductance G_{load}. Thus, a constant voltage on the capacitor representing a non-zero motion signal requires a net output current of the multiplier to maintain it. This requirement has two interesting consequences:
i) The reported optical flow is dependent on the spatial gradients (contrast). A single uncoupled cell according to Figure 2 has a steady state solution with

$$U_{i,j} \sim \frac{-E_{t_{i,j}}E_{x_{i,j}}}{(G_{load} + E_{x_{i,j}}^2 + E_{y_{i,j}}^2)} \quad \text{and} \quad V_{i,j} \sim \frac{-E_{t_{i,j}}E_{y_{i,j}}}{(G_{load} + E_{x_{i,j}}^2 + E_{y_{i,j}}^2)}$$

respectively. For the same object speed, the chip reports higher velocity signals for higher spatial gradients. Preferably, G_{load} should be as low as possible to minimize its influence on the solution.
ii) On the other hand, the locally ill-posed problem is now well-posed because G_{load} imposes a second constraint. Thus, the chip behaves sensibly in the case of low contrast input (small gradients), reporting zero motion where otherwise, unreliable high values would occur. This is convenient because the signal-to-noise ratio at low contrast is very poor. Furthermore, a single cell is forced to report the velocity on the constraint line with smallest absolute value, which is normal to the spatial gradient. That means that the chip

reports *normal flow* when there is no neighbor connection. Since there is an trade-off between the robustness of the optical flow computation and a low conductance G_{load}, the follower-connected transconductance amplifier in our implementation allows us to control G_{load} above its small intrinsic value.

4.2 Results

The results reported below were obtained from a MOSIS tinychip containing a 7x7 array of motion cells each 325x325 λ^2 in size. The chip was fabricated in 1.2 μm technology at AMI.

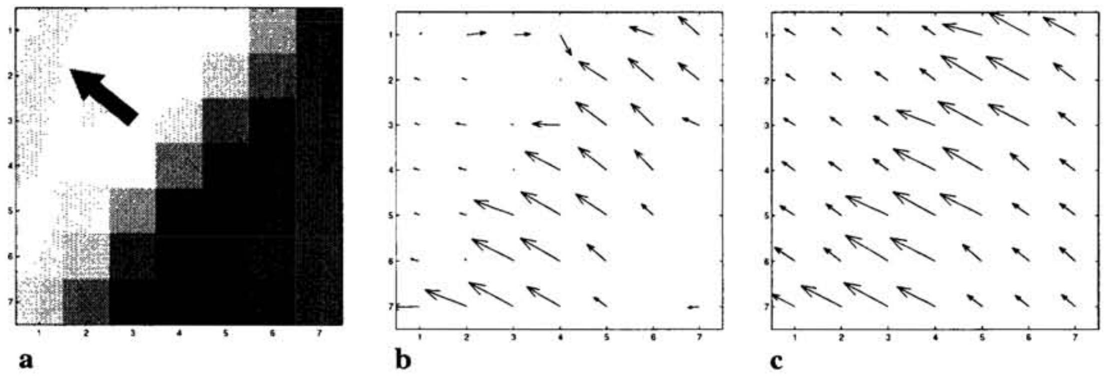

Figure 4: Smooth optical flow response of the chip to an left-upwards moving edge. **a**: photoreceptor output, the arrow indicates the actual motion direction. **b**: weak coupling (small conductance G). **c**: strong coupling.

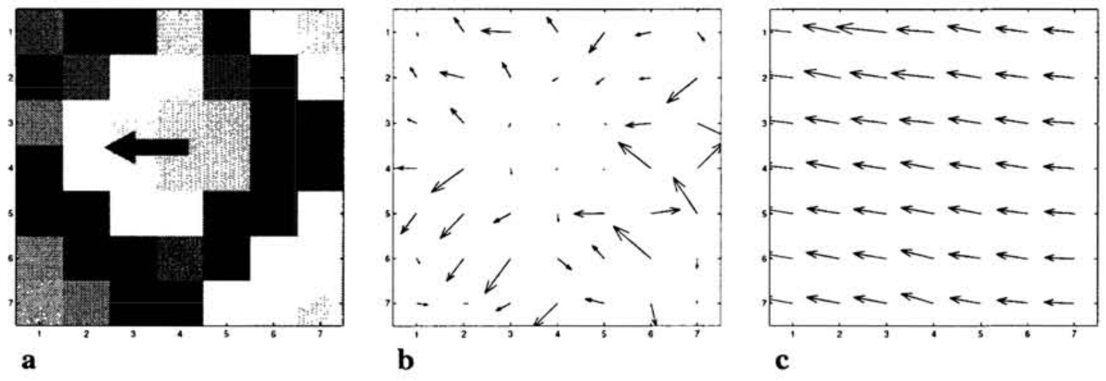

Figure 5: Response of the optical flow chip to a plaid stimulus moving towards the left: **a**: photoreceptor output; **b** shows the normal flow computation with disabled coupling between the motion cells in the network while in **c** the coupling strength is at maximum.

The chip is able to compute smooth optical flow in a qualitative manner. The smoothness can be set by adjusting the coupling conductances (Figure 4). Figure 5b presents the normal flow computation that occurs when the coupling between the motion cells is disabled. The limited resolution of this prototype chip together with the small size of the stimulus leads to a noisy response. However it is clear that the chip perceives the two gratings as separate moving objects with motion normal to their edge orientation. When the network conductance is set very high the chip performs a collective computation solving the aperture problem under the assumption of single object motion. Figure 5c shows how the chip can compute the correct motion of a plaid pattern.

5 Conclusion

We have presented here an aVLSI implementation of a network that computes 2D smooth optical flow. The strength of the resistive coupling can be varied continuously to obtain different degrees of smoothing, from a purely local up to a single global motion signal. The chip ideally computes smooth optical flow in the classical definition of Horn and Schunck. Instead of using negative and complex conductances we implemented a network solution where each motion cell is performing a local constraint satisfaction task in a recurrent negative feedback loop.
It is significant that the solution of a global energy minimization task can be achieved within a network of local constraint solving cells that do not have explicit access to the global computational goal.

Acknowledgments

This article is dedicated to Misha Mahowald. We would like to thank Eric Vittoz, Jörg Kramer, Giacomo Indiveri and Tobi Delbrück for fruitful discussions. We thank the Swiss National Foundation for supporting this work and MOSIS for chip fabrication.

References

[1] J. Tanner and C.A. Mead. An integrated analog optical motion sensor. In S.-Y. Kung, R. Owen, and G. Nash, editors, *VLSI Signal Processing, 2*, page 59 ff. IEEE Press, 1986.

[2] B.K. Horn and B.G. Schunck. Determining optical flow. *Artificial Intelligence*, 17:185–203, 1981.

[3] A. Yuille. Energy functions for early vision and analog networks. *Biological Cybernetics*, 61:115–123, 1989.

[4] T. Poggio, V. Torre, and C. Koch. Computational vision and regularization theory. *Nature*, 317(26):314–319, September 1985.

[5] B. K. Horn. Parallel networks for machine vision. Technical Report 1071, MIT AI Lab, December 1988.

[6] J. Hutchinson, C. Koch, J. Luo, and C. Mead. Computing motion using analog and binary resistive networks. *Computer*, 21:52–64, March 1988.

[7] T. Poggio, W. Yang, and V. Torre. Optical flow: Computational properties and networks, biological and analog. *The Computing Neuron*, pages 355–370, 1989.

[8] J.G. Harris, C. Koch, E. Staats, and J. Luo. Analog hardware for detecting discontinuities in early vision. *Int. Journal of Computer Vision*, 4:211–223, 1990.

[9] J. Wyatt. Little-known properties of resistive grids that are useful in analog vision chip designs. In C. Koch and H. Li, editors, *Vision Chips: Implementing Vision Algorithms with Analog VLSI Circuits*, pages 72–89. IEEE Computer Society Press, 1995.

[10] S.C. Liu. Silicon retina with adaptive filtering properties. In *Advances in Neural Information Processing Systems 10*, November 1997.

Scheduling Straight-Line Code Using Reinforcement Learning and Rollouts

Amy McGovern and Eliot Moss
{amy|moss@cs.umass.edu}
Department of Computer Science
University of Massachusetts, Amherst
Amherst, MA 01003

Abstract

The execution order of a block of computer instructions can make a difference in its running time by a factor of two or more. In order to achieve the best possible speed, compilers use heuristic schedulers appropriate to each specific architecture implementation. However, these heuristic schedulers are time-consuming and expensive to build. In this paper, we present results using both rollouts and reinforcement learning to construct heuristics for scheduling basic blocks. The rollout scheduler outperformed a commercial scheduler, and the reinforcement learning scheduler performed almost as well as the commercial scheduler.

1 Introduction

Although high-level code is generally written as if it were going to be executed sequentially, many modern computers are pipelined and allow for the simultaneous issue of multiple instructions. In order to take advantage of this feature, a scheduler needs to reorder the instructions in a way that preserves the semantics of the original high-level code while executing it as quickly as possible. An efficient schedule can produce a speedup in execution of a factor of two or more. However, building a scheduler can be an arduous process. Architects developing a new computer must manually develop a specialized instruction scheduler each time a change is made in the proposed system. Building a scheduler automatically can save time and money. It can allow the architects to explore the design space more thoroughly and to use more accurate metrics in evaluating designs.

Moss et al. (1997) showed that supervised learning techniques can induce excellent basic block instruction schedulers for the Digital Alpha 21064 processor. Although all of the supervised learning methods performed quite well, they shared several limitations. Supervised learning requires exact input/output pairs. Generating these training pairs requires an optimal scheduler that searches every valid permutation of the instructions within a basic block and saves the optimal permutation (the schedule with the smallest running time). However, this search was too time-consuming to perform on blocks with more than 10 instructions, because optimal instruction scheduling is NP-hard. Using a semi-supervised method such as reinforcement learning or rollouts does not require generating training pairs, so the method can be applied to larger basic blocks and can be trained without knowing optimal schedules.

2 Domain Overview

Moss et al. (1997) gave a full description of the domain. This study presents an overview, necessary details, our experimental method and detailed results for both rollouts and reinforcement learning.

We focused on scheduling *basic blocks* of instructions on the 21064 version (DEC, 1992) of the Digital Alpha processor (Sites, 1992). A basic block is a set of instructions with a single entry point and a single exit point. Our schedulers could reorder instructions within a basic block but could not rewrite, add, or remove any instructions. The goal of each scheduler is to find a least-cost valid ordering of the instructions. The cost is defined as the simulated execution time of the block. A valid ordering is one that preserves the semantically necessary ordering constraints of the original code. We insure validity by creating a dependency graph that directly represents those necessary ordering relationships. This graph is a directed acyclic graph (DAG).

The Alpha 21064 is a dual-issue machine with two different execution pipelines. Dual issue occurs only if a number of detailed conditions hold, e.g., the two instructions match the two pipelines. An instruction can take anywhere from one to many tens of cycles to execute. Researchers at Digital have a publicly available 21064 simulator that also includes a heuristic scheduler for basic blocks. We call that scheduler *DEC*. The simulator gives the running time for a given scheduled block assuming all memory references hit the cache and all resources are available at the beginning of the block. All of our schedulers used a greedy algorithm to schedule the instructions, i.e., they built schedules sequentially from beginning to end with no backtracking.

In order to test each scheduling algorithm, we used the 18 SPEC95 benchmark programs. Ten of these programs are written in FORTRAN and contain mostly floating point calculations. Eight of the programs are written in C and focus more on integer, string, and pointer calculations. Each program was compiled using the commercial Digital compiler at the highest level of optimization. We call the schedules output by the compiler *ORIG*. This collection has 447,127 basic blocks, containing 2,205,466 instructions.

3 Rollouts

Rollouts are a form of Monte Carlo search, first introduced by Tesauro and Galperin (1996) for use in backgammon. Bertsekas et al. (1997a,b) have explored rollouts in other domains and proven important theoretical results. In the instruction scheduling domain, rollouts work as follows: suppose the scheduler comes to a point where it has a partial schedule and a set of (more than one) candidate instructions to add to the schedule. For each candidate, the scheduler appends it to the partial schedule and then follows a fixed policy π to schedule the remaining instructions. When the schedule is complete, the scheduler evaluates the running time and returns. When π is stochastic, this rollout can be repeated many times for each instruction to achieve a measure of the average expected outcome. After rolling out each candidate, the scheduler picks the one with the best average running time.

Our first set of rollout experiments compared three different rollout policies π. The theory developed by Bertsekas et al. (1997a,b) proved that if we used the DEC scheduler as π, we would perform no worse than DEC. An architect proposing a new machine might not have a good heuristic available to use as π, so we also considered policies more likely to be available. The first was the random policy, *RANDOM-*π, which is a choice that is clearly always available. Under this policy, the rollout makes all choices randomly. We also used the ordering produced by the optimizing compiler ORIG, denoted *ORIG-π*. The last rollout policy tested was the DEC scheduler itself, denoted *DEC-π*.

The scheduler performed only one rollout per candidate instruction when using ORIG-π and DEC-π because they are deterministic. We used 25 rollouts for RANDOM-π. After performing a number of rollouts for each candidate instruction, we chose the instruction with the best average running time. As a baseline scheduler, we also scheduled each block randomly. Because the running time increases quadratically with the number of rollouts, we focused our rollout experiments on one program in the SPEC95 suite: *applu*.

Table 1 gives the performance of each rollout scheduler as compared to the DEC scheduler on all 33,007 basic blocks of size 200 or less from applu. To assess the performance of each rollout policy π, we used the ratio of the weighted execution time of the rollout scheduler to the weighted execution time of the DEC scheduler. More concisely, the performance measure was:

$$\text{ratio} = \frac{\sum_{\text{all blocks}} \text{rollout scheduler execution time} * \text{number of times block is executed}}{\sum_{\text{all blocks}} \text{DEC scheduler execution time} * \text{number of times block is executed}}$$

This means that a faster running time on the part of our scheduler would give a smaller ratio.

Scheduler	Ratio	Scheduler	Ratio
Random	1.3150	RANDOM-π	1.0560
ORIG-π	0.9895	DEC-π	0.9875

Table 1: Ratios of the weighted execution time of the rollout scheduler to the DEC scheduler. A ratio of less than one means that the rollouts outperformed the DEC scheduler.

All of the rollout schedulers far outperformed the random scheduler which was 31% slower than DEC. By only adding rollouts, RANDOM-π was able to achieve a running time only 5% slower than DEC. Only the schedulers using ORIG-π and DEC-π as a model outperformed the DEC scheduler. Using ORIG-π and DEC-π for rollouts produced a schedule that was 1.1% faster than the DEC scheduler on average. Although this improvement may seem small, the DEC scheduler is known to make optimal choices 99.13% of the time for blocks of size 10 or less (Stefanović, 1997).

Rollouts were tested only on applu rather than on the entire SPEC95 benchmark suite due to the lengthy computation time. Rollouts are costly because performing m rollouts on n instructions is $O(n^2m)$, whereas a greedy scheduling algorithm is $O(n)$. Again, because of the time required, we only performed five runs of RANDOM-π. Since DEC-π and ORIG-π are deterministic, only one run was necessary. We also ran the random scheduler 5 times. Each number reported above is the geometric mean of the ratios across the five runs.

Part of the motivation behind using rollouts in a scheduler is to obtain fast schedules without spending the time to build a precise heuristic. With this in mind, we explored RANDOM-π more closely in a follow-up experiment.

Evaluation of the number of rollouts

This experiment considered how performance varies with the number of rollouts. We tested 1, 5, 10, 25, and 50 rollouts per candidate instruction. We also varied the metric for choosing among candidates. Instead of always choosing the instruction with the best average performance, we also experimented with selecting the instruction with the absolute best running time among its rollouts. We hypothesized that selection of the absolute best path might lead to better performance overall. These experiments were performed on all 33,007 basic blocks of size 200 or less from applu.

Figure 1 shows the performance of the rollout scheduler as a function of the number of rollouts. Performance is assessed in the same way as before: ratio of weighted execution

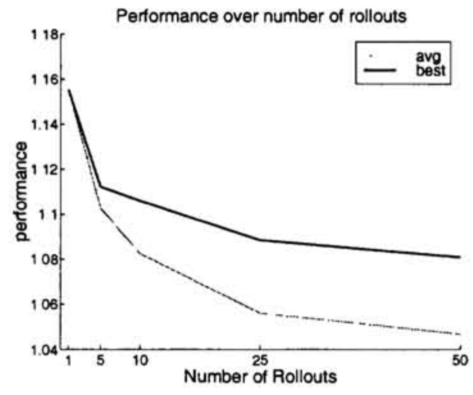

Figure 1: Performance of rollout scheduler with the random model as a function of the number of rollouts and the choice of evaluation function.

times. Thus, a lower number is better. Each data point represents the geometric mean over five different runs. The difference in performance between one rollout and five rollouts using the average choice for each rollout is 1.16 versus 1.10. However, the difference between 25 rollouts and 50 rollouts is only 1.06 versus 1.05. This indicates the tradeoff between schedule quality and the number of rollouts. Also, choosing the instructions with the best rollout schedule did not yield better performance over any numbers of rollouts. We hypothesize that this is due to the stochastic nature of the rollouts. Once the scheduler chooses an instruction, it repeats the rollout process again. By choosing the instruction with the absolute best rollout, there is no guarantee that the scheduler will find that permutation of instructions again on the next rollout. When it chooses the instruction with the best average rollout, the scheduler has a better chance of finding a good schedule on the next rollout.

Although the rollout schedulers performed quite well, the extremely long scheduling time is a major drawback. Using 25 rollouts per block took over 6 hours to schedule one program. Unless this aspect can be improved, rollouts cannot be used for all blocks in a commercial scheduler or in evaluating more than a few proposed machine architectures. However, because rollout scheduling performance is high, rollouts could be used to optimize the schedules on important (long running times or frequently executed) blocks within a program.

4 Reinforcement Learning Results

4.1 Overview

Reinforcement learning (RL) is a collection of methods for discovering near-optimal solutions to stochastic sequential decision problems (Sutton & Barto, 1998). A reinforcement learning system does not require a teacher to specify correct actions. Instead, the learning agent tries different actions and observes their consequences to determine which actions are best. More specifically, in the reinforcement learning framework, a learning *agent* interacts with an *environment* over a series of discrete time steps $t = 0, 1, 2, 3, \ldots$. At each time t, the agent is in some *state*, denoted s_t, and chooses an action, denoted a_t, which causes the environment to transition to state s_{t+1} and to emit a reward, denoted r_{t+1}. The next state and reward depend only on the preceding state and action, but they may depend on it in a stochastic fashion. The objective is to learn a (possibly stochastic) mapping from states to actions called a *policy*, which maximizes the cumulative discounted reward received by the agent. More precisely, the objective is to choose action a_t so as to maximize the expected *return*, $\mathrm{E}\left\{\sum_{i=0}^{\infty} \gamma^i r_{t+i+1}\right\}$, where $\gamma \in [0, 1)$ is a discount-rate parameter.

A common solution strategy is to approximate the *optimal value function* V^*, which maps states to the maximal expected return that can be obtained starting in each state and taking the best action. In this paper we use *temporal difference (TD) learning* (Sutton, 1988). In this method, the approximation to V^* is represented by a table with an entry $V(s)$ for every state. After each transition from state s_t to state s_{t+1}, under an action with reward r_{t+1}, the estimated value function $V(s_t)$ is updated by:

$$V(s_t) \leftarrow V(s_t) + \alpha\left[r_{t+1} + \gamma V(s_{t+1}) - V(s_t)\right]$$

where α is a positive step-size parameter.

4.2 Experimental Results

Scheeff et al. (1997) have previously experimented with reinforcement learning in this domain. However, the results were not as good as hoped. Finding the right reward structure was the difficult part of using RL in this domain. Rewarding based on number of cycles to execute the block does not work well as it punishes the learner on long blocks. To normalize for this effect, Scheeff et al. (1997) rewarded based on the cycles per instruction (CPI). However, learning with this reward also did not work well as some blocks have more unavoidable idle time than others. A reward based solely on CPI does not account for this aspect. To account for this variation across blocks, we gave the RL scheduler a final reward of:

$$r = \text{time to execute block} - \max\left(\text{minimum weighted critical path}, \left(\frac{\text{\# of instructions}}{2}\right)\right)$$

The scheduler received a reward of zero unless the schedule was complete. As the 21064 processor can only issue two instructions at a time, the number of instructions divided by 2 gives an absolute lower bound on the running time. The weighted critical path (wcp) helps to solve the problem of the same size blocks being easier or harder to schedule than others. When a block is harder to execute than another block of the same size, the wcp tends to be higher, thus causing the learner to get a different reward. The wcp is correlated with the predicted number of execution cycles for the DEC scheduler ($r = 0.9$) and the number of instructions divided by 2 is also correlated ($r = 0.78$) with the DEC scheduler. Future experiments will use a weighted combination of these two features to compute the reward.

As with the supervised learning results presented in Moss et al. (1997), the RL system learned a preferential value function between candidate instructions. That is, instead of learning the value of instruction A or instruction B, RL learned the value of choosing instruction A over instruction B. The state space consisted of a tuple of features from a current partial schedule and the two candidate instructions. These features were derived from knowledge of the DEC simulator. The features and our intuition for their importance are summarized in Table 2.

Previous experiments (Moss et al. 1997) showed that the actual value of wcp and e did not matter as much as their relative values. Thus, for those features we used the signum (σ) of the difference of their values for the two candidate instruction. Signum returns $-1, 0,$ or 1 depending on whether the value is less than, equal to, or greater than zero. Using this representation, the RL state space consisted of the following tuple, given candidate instruction x and y and partial schedule p:

$$\text{state\_vec}(p, x, y) = \langle \text{odd}(p), \text{ic}(x), \text{ic}(y), \text{d}(x), \text{d}(y), \sigma(\text{wcp}(x) - \text{wcp}(y)), \sigma(\text{e}(x) - \text{e}(y))\rangle$$

This yields 28,800 unique states. Figure 2 shows an example partial schedule, a set of candidate instructions, and the resulting states for the RL system.

The RL scheduler does not learn over states where there are no choices to be made. The last choice point in a trajectory is given the final reward even if further instructions are scheduled from that point. The values of multiple states are updated at each time step because the instruction that is chosen affects the preference function of multiple states. For

Heuristic Name	Heuristic Description	Intuition for Use
Odd Partial (odd)	Is the current number of instructions scheduled odd or even?	If TRUE, we're interested in scheduling instructions that can dual-issue with the previous instruction.
Instruction Class (ic)	The Alpha's instructions can be divided into equivalence classes with respect to timing properties.	The instructions in each class can be executed only in certain execution pipelines, etc.
Weighted Critical Path (wcp)	The height of the instruction in the DAG (the length of the longest chain of instructions dependent on this one), with edges weighted by expected latency of the result produced by the instruction	Instructions on longer critical paths should be scheduled first, since they affect the lower bound of the schedule cost.
Actual Dual (d)	Can the instruction dual-issue with the previous scheduled instruction?	If Odd Partial is TRUE, it is important that we find an instruction, if there is one, that can issue in the same cycle with the previous scheduled instruction.
Max Delay (e)	The earliest cycle when the instruction can begin to execute, relative to the current cycle; this takes into account any wait for inputs for functional units to become available	We want to schedule instructions that will have their data and functional unit available earliest.

Table 2: Features for Instructions and Partial Schedule

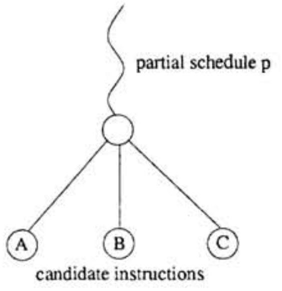

States for RL system

State label	State
AB	state_vec(p,A,B)
AC	state_vec(p,A,C)
BC	state_vec(p,B,C)
BA	state_vec(p,B,A)
CA	state_vec(p,C,A)
CB	state_vec(p,C,B)

Figure 2: On the left is a graphical depiction of a partial schedule and three candidate instructions. The table on the right shows how the RL system makes its states from this.

example, using the partial schedule and candidate instructions shown in Figure 2, scheduling instruction A, the RL system would backup values for AB, AC, and the opposite values for BA and CA.

Using this system, we performed leave-one-out cross validation across all blocks of the SPEC95 benchmark suite. Blocks with more than 800 instructions were broken into blocks of 800 or less because of memory limitations on the DEC simulator. This was true for only two applications: applu and fpppp. The RL system was trained online for 19 of the 20 applications using $\alpha = 0.05$ and an ϵ-greedy exploration method with $\epsilon = 0.05$. This was repeated 20 different times, holding one program from SPEC95 out of the training each time. We then evaluated the greedy policy ($\epsilon = 0$) learned by the RL system on each program that had been held out. All ties were broken randomly. Performance was assessed the same way as before. The results for each benchmark are shown in Table 3. Overall, the RL scheduler performed only 2% slower than DEC. This is a geometric mean over all applications in the suite and on all blocks. Although the RL system did not outperform the DEC scheduler overall, it significantly outperformed DEC on the large blocks (applu-big and fpppp-big).

5 Conclusions

The advantages of the RL scheduler are its performance on the task, its speed, and the fact that it does not rely on any heuristics for training. Each run was much faster than with rollouts and the performance came close to the performance of the DEC scheduler. In a

App	Ratio	App	Ratio	App	Ratio	App	Ratio
applu	1.001	*applu-big*	*0.959*	apsi	1.018	cc1	1.022
compress95	*0.977*	fpppp	1.055	*fpppp-big*	*0.977*	go	1.028
hydro2d	1.022	*ijpeg*	*0.975*	li	1.012	m88ksim	1.042
mgrid	1.009	perl	1.014	su2cor	1.018	swim	1.040
tomcatv	1.019	turb3d	1.218	vortex	1.032	wave5	1.032

Table 3: Performance of the greedy RL-scheduler on each application in SPEC95 over all leave-one-out cross-validation runs as compared to DEC. Applications whose running time was better than DEC are shown in italics.

system where multiple architectures are being tested, RL could provide a good scheduler with minimal setup and training.

We have demonstrated two methods of instruction scheduling that do not rely on having heuristics and that perform quite well. Future work could address tying the two methods together while retaining the speed of the RL learner, issues of global instruction scheduling, scheduling loops, and validating the techniques on other architectures.

Acknowledgments

We thank John Cavazos and Darko Stefanović for setting up the simulator and for prior work in this domain, along with Paul Utgoff, Doina Precup, Carla Brodley, and David Scheeff. We also wish to thank Andrew Barto, Andrew Fagg, and Doina Precup for comments on earlier versions of the paper. This work is supported in part by the National Physical Science Consortium, Lockheed Martin, Advanced Technology Labs, and NSF grant IRI-9503687 to Roderic A. Grupen and Andrew G. Barto. We thank various people of Digital Equipment Corporation, for the DEC scheduler and the ATOM program instrumentation tool (Srivastava & Eustace, 1994), essential to this work. We also thank Sun Microsystems and Hewlett-Packard for their support.

References

Bertsekas, D. P. (1997). Differential training of rollout policies. In *Proc. of the 35th Allerton Conference on Communication, Control, and Computing*. Allerton Park, Ill.

Bertsekas, D. P., Tsitsiklis, J. N. & Wu, C. (1997). Rollout algorithms for combinatorial optimization. *Journal of Heuristics*.

DEC (1992). *DEC chip 21064-AA Microprocessor Hardware Reference Manual* (first edition Ed.). Maynard, MA: Digital Equipment Corporation.

Moss, J. E. B., Utgoff, P. E., Cavazos, J., Precup, D., Stefanović, D., Brodley, C. E. & Scheeff, D. T. (1997). Learning to schedule straight-line code. In *Proceedings of Advances in Neural Information Processing Systems 10 (Proceedings of NIPS'97)*. MIT Press.

Scheeff, D., Brodley, C., Moss, E., Cavazos, J. & Stefanović, D. (1997). Applying reinforcement learning to instruction scheduling within basic blocks. Technical report, University of Massachusetts, Amherst.

Sites, R. (1992). *Alpha Architecture Reference Manual*. Maynard, MA: Digital Equipment Corporation.

Srivastava, A. & Eustace, A. (1994). ATOM: A system for building customized program analysis tools. In *Proc. ACM SIGPLAN '94 Conf. on Prog. Lang. Design and Impl.* (pp. 196–205).

Stefanović, D. (1997). The character of the instruction scheduling problem. University of Massachusetts, Amherst.

Sutton, R. S. (1988). Learning to predict by the method of temporal differences. *Machine Learning*, *3*, 9–44.

Sutton, R. S. & Barto, A. G. (1998). *Reinforcement Learning. An Introduction*. Cambridge, MA: MIT Press.

Tesauro, G. & Galperin, G. R. (1996). On-line policy improvement using monte-carlo search. In *Advances in Neural Information Processing: Proceedings of the Ninth Conference*. MIT Press.